Journal of MATERIALS RESEARCH

Article
DOI:10.1557/s43578-022-00631-0

Effects of initial microstructure on the aging behavior and subsequent mechanical properties of Ti–Nb–O titanium alloy

Junshuai Wang[1], Wenlong Xiao[1,3,a)], Yu Fu[1], Lei Ren[1], Bo Song[1], Cuiyun Liu[2], Chaoli Ma[1,2]

[1] Key Laboratory of Aerospace Advanced Materials and Performance of Ministry of Education, School of Materials Science and Engineering, Beihang University, Beijing 100191, China
[2] Research Institute for Frontier Science, Beihang University, Beijing 100191, China
[3] Yunnan Innovation Institute of Beihang University, Kunming 650000, Yunnan, China
[a)] Address all correspondence to this author. e-mail: wlxiao@buaa.edu.cn

Received: 18 February 2022; accepted: 14 June 2022; published online: 28 June 2022

Metastable β-type Ti–38Nb–0.2O alloy was subjected to cold rolling (CR) and solution treatment (ST), and the effects of initial microstructure on the aging behavior and subsequent mechanical properties were investigated. High density of dislocations and grain refinement were introduced by CR, which suppressed the *ω* phase and promoted the *α* phase in the subsequent aging process. Upon aging at 573 K, the CR specimen consisted of *α* + *β* phase and high density of dislocations, while the ST specimen showed homogeneous precipitation of *ω* phase. Upon aging at 773 K, the CR specimen exhibited ultrafine equiaxed *α* phase without obvious *β* grain boundary, while the ST specimen contained acicular *α* precipitates nonuniformly distributed in the internal grain and grain boundary, and precipitate-free zone near grain boundaries were observed. The different initial microstructures led to large difference in strength and Young's modulus between the aged specimens.

Introduction

Metastable β-type Ti–Nb based titanium alloys have attracted considerable research and development efforts thanks to unique biocompatibility as well as balanced mechanical properties and outstanding corrosion resistance, which are the one of the most promising for biomedical applications [1, 2]. However, the Ti–Nb alloys with a single *β* phase normally exhibit low strength, which limits their applications. In general, the heat treatment can substantially enhance mechanical properties of Ti alloys, through regulating *α* and/or *ω* phase precipitate, grain size, texture and so on. For example, Zhang et al. employed short-time heat treatment to form *ω* and *α* precipitates in Ti–12Mo alloy and therefore improved the yield strength [3]. Through heat treatment, the nano-sized network of lamellar *α* phase was obtained in Ti–24Nb–4Zr–7.9Sn alloy, which suppressed the stress-induced martensitic transformation and increased the yield strength [4]. However, the precipitation of *ω* and *α* phases may have some adverse effects on other properties. The isothermal *ω* phase will reduce the ductility and evidently increase the modulus of Ti alloys, which is undesirable for biomedical applications [5]. The continuous grain boundary *α* layers also could lead to low ductility and intergranular failure [6]. To satisfy the highly desirable for high strength and low modulus meanwhile as much as possible, many researches focused on suppressing the deleterious *ω* phase and promoting homogeneous precipitation of fine *α* phase [7].

The precipitation of the secondary phase in Ti alloys is affected by many factors, such as aging temperature, heating rate, and initial microstructure before the aging treatment [8, 9]. Generally, *ω* phase tends to precipitate at a low aging temperature, while *α* phase tends to precipitate at a higher aging temperature [10]. Besides, the substructure introduced by plastic deformation also has a substantial influence on *α* and *ω* precipitation. It has been reported that the sub-grain boundary and dislocations can lead to much more uniform intragranular *α* precipitates due to preferentially heterogeneous nucleation [11]. In addition, they also caused the morphology of *α* phase to change from acicular to equiaxed after aging treatment [12] or retard the precipitation of *ω* phase [13]. Guo et al. suggested that the dislocation tangles introduced by cold rolling (CR) block

the movements of dislocations which are necessary for the ω transformation from β, and thus give the Ti–25Nb–2Mo–4Sn alloy high strength and low Young's modulus after annealing treatment [14, 15]. The Ti–24Nb (at.%) after CR and solution treatment (ST) displayed apparent different phase transformation behaviors, in which the CR condition underwent both the β to α'' and β to ω transformations when cooling from 350 to − 196 °C, while only the β to ω transformation was observed in the ST condition [8]. Therefore, it is meaningful to gain an in-depth understanding of the relationship between processing routes and resulting microstructures to optimize the mechanical properties of metastable Ti alloys.

The interstitial oxygen has strong solid strengthening effect, which could effectively increase the strength of Ti alloys [16]. Besides, the oxygen has a great effect on the phase transformation, even at very low concentrations. It has been reported that the addition of oxygen increased the α/β transus temperature by 200 K/at.% O and decreased the martensitic transformation starts temperature (Ms) by 160 K/at.% O [17]. Therefore, the 38Nb–0.2O (wt%) alloy was selected as a research object due to its higher strength compared with Ti–38Nb alloys and single β structure in the solid solution state. In this study, the Ti–38Nb–0.2O (wt%) alloy subjected to CR or ST was aged at different temperatures. The purpose of this study was to provide insight into the influence of the initial microstructure before aging treatments on the α and ω precipitation behavior and corresponding mechanical properties to optimize the mechanical properties of metastable β Ti alloy for biomedical applications.

Results

Initial microstructure

Figure 1 shows the optical micrographs displaying the microstructure and corresponding XRD profiles of CR and ST specimens. Figure 1(a) shows the optical images of the CR specimen viewed on the longitudinal section. An apparent fibrous stripe structure parallel to the rolling direction could be observed due to the severe cold deformation. When viewed on the transverse section [Fig. 1(b)], a swirled marble-like microstructure is visible. Such swirled marble-like structure is typically observed in β-type Ti alloys after cold processing, such as Gum Metal [18], Ti–24Nb–4Zr–8Sn [19] and Ti–33.6Nb–4Sn [20]. Such phenomenon has been consistently explained in terms of a peculiar dislocation evolution behavior and plane-strain deformation of the bcc crystals dominated by its inherent characteristics [19]. The XRD profile in Fig. 1(d) indicates that the CR specimen contains both β and α'' phases. The formation of α'' martensite is resulted from stress-induced martensitic transformation during CR, since the low β stability of Ti–38Nb–0.2O alloy. In addition, the widths of the diffraction peaks (FWHM) of β(110) in CR specimen (0.765) is wider than that of ST specimen (0.569). The widen of diffraction peaks for the CR specimen is resulted from the strong refinement of microstructure and high-density of lattice defects. After ST, equiaxed β grains with mean grain size of around 70 μm are observed in the ST specimen [Fig. 1(c)], and the XRD trace only shows the reflections for β phase in this state. The dislocation tangles and grain boundaries in CR specimens could be observed by TEM, as shown in Fig. 1(e). Besides, the stress-induced α'' phases also could be observed, shown in Fig. 1(f).

Microstructure after aging treatment

The CR and ST specimens showed distinct microstructure and phase constituents, which result in different microstructures after aging treatment at 573 K and 773 K. Figure 2 shows the XRD profiles of aged specimens. The CR and ST specimens aged at 573 K and 773 K are referred to as CRA-573, CRA-773, STA-573, and STA-773, respectively. It can be found that the CRA-573 specimen consists of β and α phases. In comparison with the CR specimen [Fig. 1(d)], the peaks of α'' phase are not visible due to the stress-induced α'' martensite reverting to the β phase upon heating. The peaks of the STA-573 specimen can be identified as $\beta + \omega$ phases. When increased the aging temperature, the CRA-773 and STA-773 specimens both exhibit $\alpha + \beta$ phases. It should be noted that the peak intensity of α phase in the CRA-773 specimen is higher than that in the STA-773 specimen, indicating a higher volume fraction of α phase in the CRA-773 specimen.

Figure 3 shows the optical micrographs of the aged specimens. The CRA-573 specimen exhibits a fibrous stripe structure parallel to the rolling direction similar to the CR specimen, but with a lower degree, as shown in Fig. 3(a). The STA-573 specimen shows dispersed precipitates in equiaxed β grains, but could not be distinguished due to the small-scale size and the limited OM magnification. The microstructure of the CRA-773 specimen shown in Fig. 3(c) is consisted of ultrafine grained α phase embedded by β matrix. Nevertheless, no pronounced β grain boundary could be observed. As seen in Fig. 3(d), the STA-773 specimen presents the inhomogeneous distribution of α precipitates in the internal and boundaries of β grains. And several near-grain boundaries regions are found to be the absent of α precipitates, forming a precipitate-free zone (PFZ) [21, 22].

Figure 4 shows the TEM observations of the CRA-573 and STA-573 specimens. In Fig. 4(a), the dislocation tangles introduced by cold deformation can be observed, as indicated by white arrows. Due to the low aging temperature at 573 K, the dislocation recovery is not complete. The near-continuous diffraction rings resulted from the significant grain refinement indicate that the aging treatment did not lead to apparent grain recrystallization and growth. It is worth noting that no visible reflections coming from ω phase are observed. The TEM observations of CRA-573

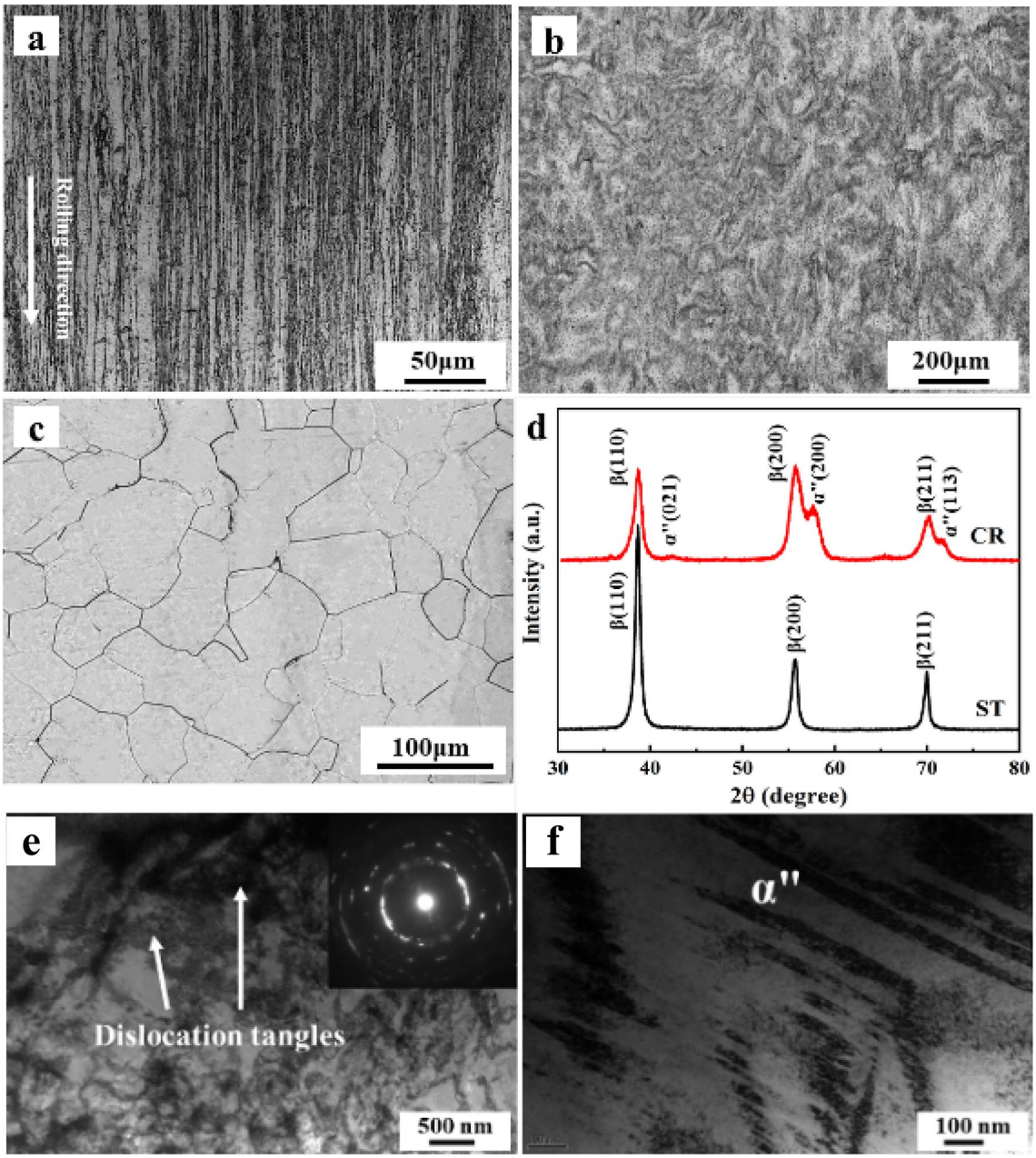

Figure 1: Optical images viewed on the longitudinal section (a) and the transverse section (b) showing the microstructure of the CR specimen, and micrograph of the ST specimen (c) showing equiaxed β grains, XRD patterns (d) showing the phase constitutions of the CR and ST specimens, TEM images of the CR specimen (e–f) showing the dislocations tangles and α'' phase.

specimen correspond to XRD results showing $\beta+\alpha$ phase constitutions. For the STA-573 specimen shown in Fig. 4(b), nanoscaled ellipsoidal precipitates are homogeneously distributed throughout the β phase matrix. These precipitates are identified as ω phase by electron diffraction, with SAED pattern taken from the $[113]_\beta$ zone axis showing additional diffraction intensity maxima at 1/3 and 2/3 $\{112\}_\beta$ position. Figure 5 shows bright-field (BF) TEM images of CRA-773 and STA-773 specimens, respectively. It is observed that the α precipitates show an equiaxed shape with an average size of about 300 nm in CRA-773 specimens. However, the α phase in the STA-773 specimen show completely different morphologies, exhibiting acicular morphology with dozens of nanometers in width and hundreds of nanometers in length.

Tensile properties

The tensile properties of alloys were determined by uniaxial tensile testing. The corresponding stress–strain curves are plotted

in Fig. 6, and the tensile properties are listed in Table 1. The plastic yielding point is defined as the stress required to generate plastic deformation and marked by dots in the stress–strain curve. For comparison, the ST specimen was also tested and plotted in Fig. 6. The ST specimen shows an obvious double yielding behavior, which is the typical deformation characteristic of metastable β-type Ti alloys [23, 24]. The first yielding corresponds to the critical stress to induce α'' martensitic transformation from the parent β phase, and the second yielding to the onset of dislocation slip [25]. As shown in Table 1, the ST specimen exhibits the lowest Young's modulus of 50 GPa, yielding strength (YS) of 484 MPa, ultimate tensile strength (UTS) of 620 MPa, and largest elongation of 46%. Compared to ST specimens, the double yielding behavior disappears in all the aged specimens, accompanying the increase of strength and the decrease of plasticity. The CRA-573 specimen exhibits the highest UTS of 1102 MPa, but the elongation significantly decreases to 7%. The STA-573 specimen shows a higher modulus of 82 GPa with total elongation of 16%. When the aging temperature increases to 773 K, the strengthening effect decreases slightly. The UTS of CRA-773 and STA-773 specimens are 794 MPa and 736 MPa, respectively. And Young's modulus of the STA-773 specimen slightly increases to 56 GPa, compared to the ST specimen. As listed in Table 1, the hardness of specimens has a similar increase tendency with strength. The specimens after aging at low temperatures have higher hardness.

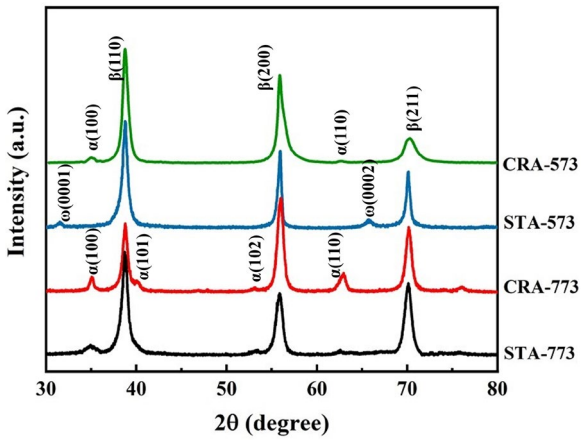

Figure 2: XRD patterns of the aged specimens with different pre-treatments.

It's noteworthy that the STA-773 specimen shows peculiar nonlinear deformation behavior accompanied by decreased elastic modulus with an increasing elastic strain called "elastic softening". The similar deformation behavior has been observed in other metastable β-Ti alloys, which is suggested to result from the nanodomain that inhibits the stress-induced long-ranged martensitic transformation [26], localized deformations induced by plastic instability originating [27], reversible nanodisturbances and homogeneously generated dislocation loop [28], and dislocation-free plastic deformation [18].

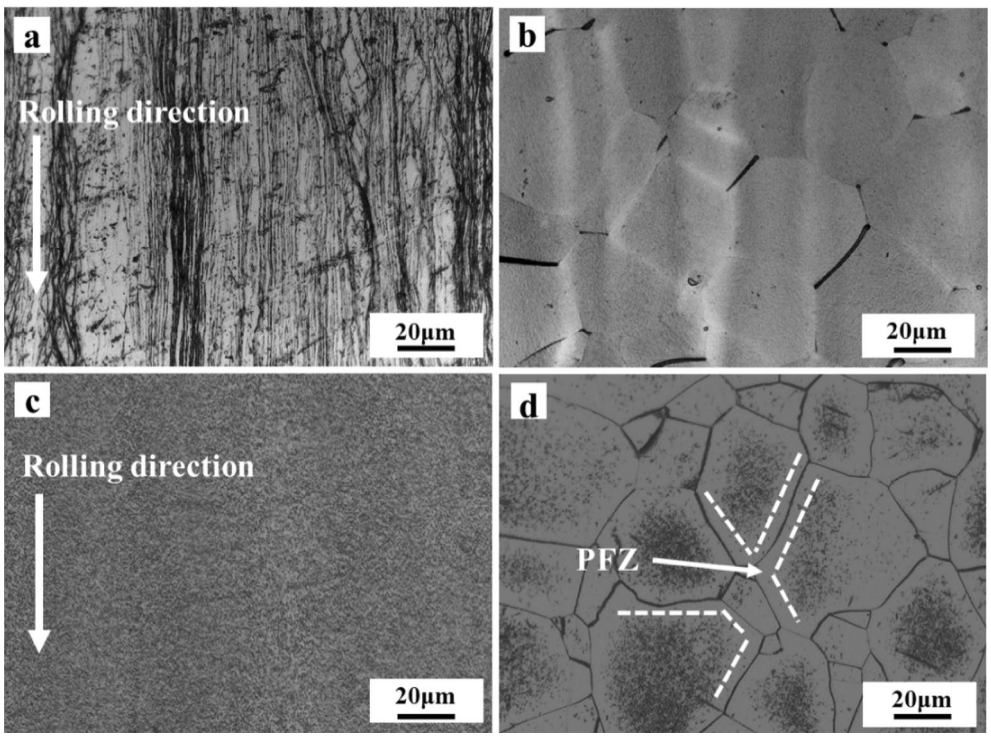

Figure 3: OM images of the aged specimens: (a) CRA-573, (b) STA-573, (c) CRA-773, (d) STA-773.

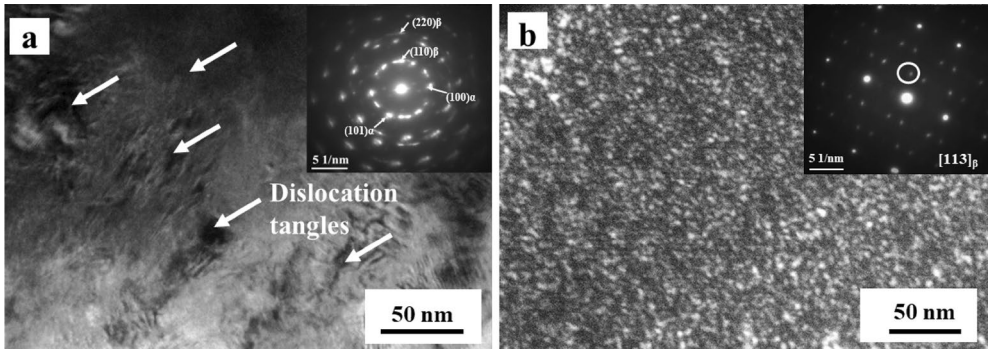

Figure 4: TEM micrographs of the specimens aged at 573 K: (a) Bright-field image of the CRA-573 specimen and SAED pattern (inset); (b) Dark-field image of the ω phase of STA-573 specimen and SAED pattern (inset).

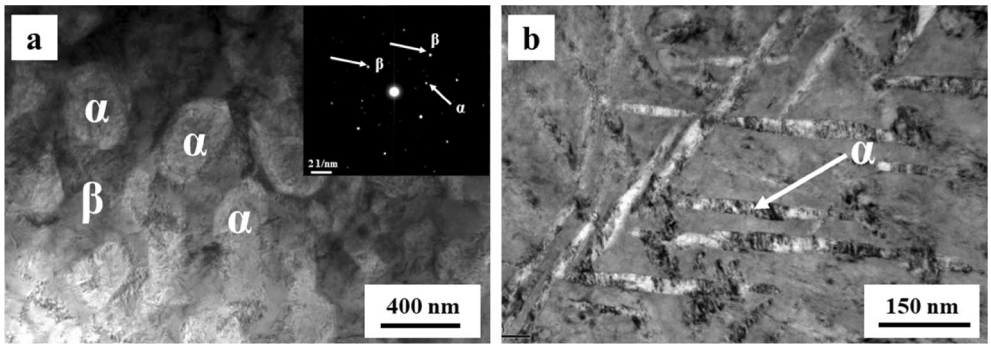

Figure 5: TEM micrographs of the specimens aged at 773 K: (a) Bright-field image of the CRA-773 specimen; (b) Bright-field image of the STA-773 specimen.

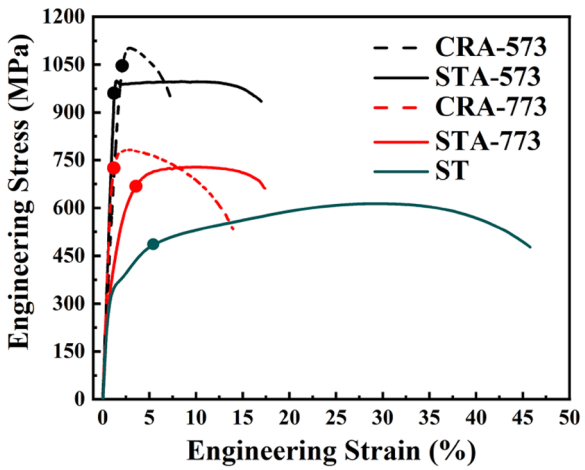

Figure 6: Engineering stress–strain curves of the aged specimens with different initial microstructures.

TABLE 1: Mechanical properties of Ti–38Nb–0.2O alloy under different states.

State	E (GPa)	YS (MPa)	UTS (MPa)	EL (%)	HV
ST	49 ± 3	484 ± 37	620 ± 65	46 ± 4	191 ± 6
CRA-573	60 ± 3	1051 ± 67	1102 ± 77	7 ± 2	290 ± 13
STA-573	82 ± 2	998 ± 35	1008 ± 52	16 ± 2	328 ± 11
CRA-773	78 ± 1	738 ± 26	794 ± 34	14 ± 1	208 ± 9
STA-773	56 ± 3	692 ± 24	736 ± 41	17 ± 2	201 ± 7

Discussions

The results reveal that the initial state (CR and ST) significantly affects the microstructure evolution in the subsequent aging process, which eventually affects the mechanical properties of the alloy. Cold work has been proved to produce an obvious local region with dislocation and grain refinement [29]. Below we will discuss the effect of lattice defects induced by CR on ω and α precipitation and the effect of precipitation on mechanical properties.

Effect of initial microstructure on the aging behavior

The α and ω phases are predominant precipitates in metastable β Ti alloys, which significantly affect the mechanical properties. Their precipitations are affected by many factors, including aging temperature, time, β stability of matrix, and lattice defects [30]. Generally, ω phase tends to precipitate at a lower temperature,

while α phase tends to precipitate at a higher aging temperature [10]. Figure 7 summarizes schematically the microstructure evolution in the aging process with different initial microstructures.

It has been reported that the ω structure forms involving the collapse of {111} planes in the [111] direction in β phase. And based on the dislocation mechanisms, the ω transformation can be attributed to the movements of 1/3[111] and 1/12[111] dislocations inhomogeneous shear in consecutive {211} planes [31]. This means that the factors hindering the movement of dislocation could suppress the formation of ω phase [13]. In general, the dislocation tangles and grain boundaries can hamper the movements of dislocation [32]. As shown in Fig. 1, high-density dislocation and grain boundaries caused by CR are observed in the CR specimen. Therefore, the precipitation of ω phase is suppressed during aging at 573 K due to the dislocation tangles and grain boundaries in CR specimens. Whereas in ST state, the specimens undergo complete recrystallization without apparent dislocation tangles in the coarse grain. Therefore, the movements of 1/3[111] and 1/12[111] dislocations necessary for the formation of ω can

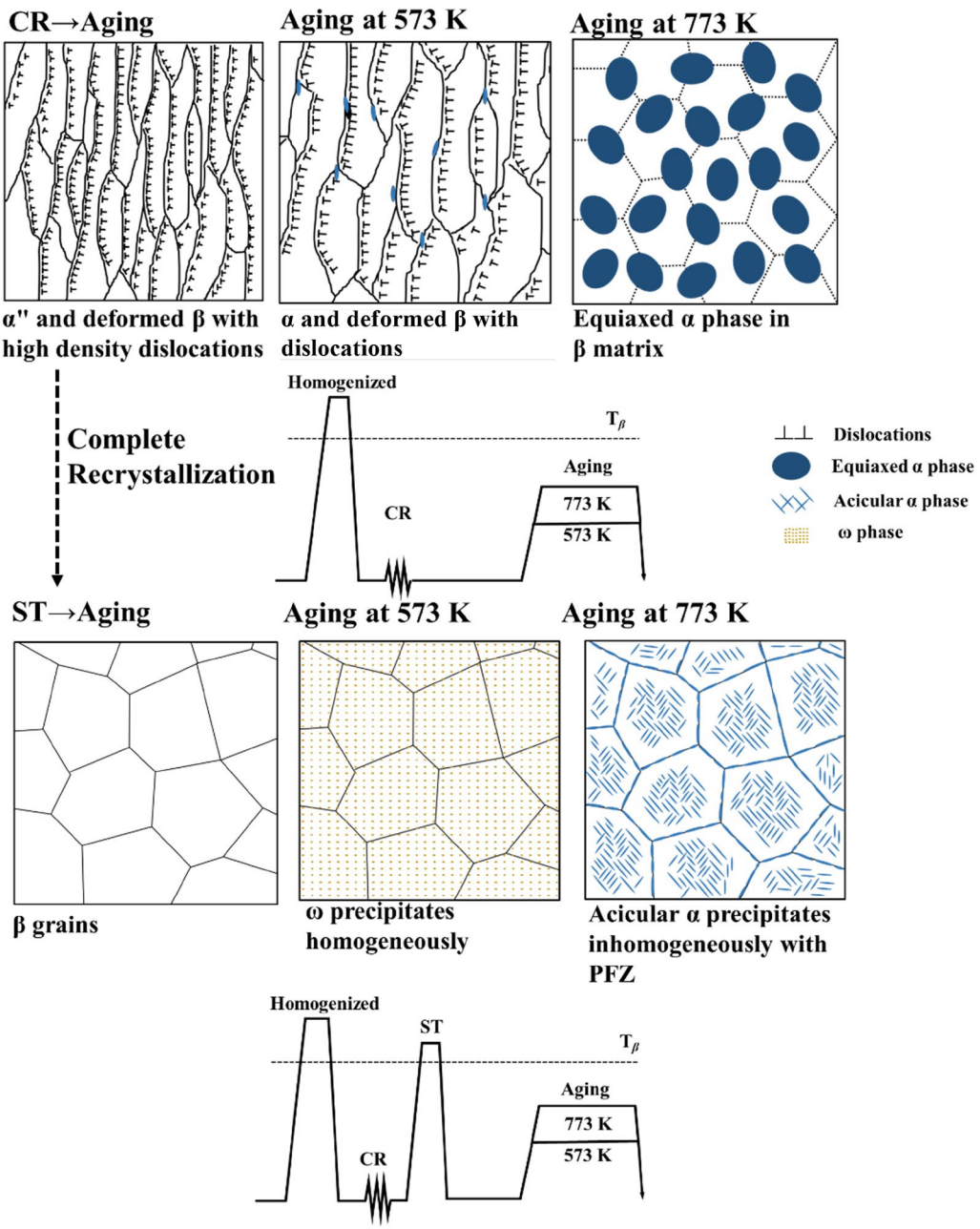

Figure 7: Schematic illustration showing the microstructure evolution in aging process.

be easily achieved and a lot of ω precipitates form in β matrix, as shown in Fig. 4(b).

As is well known, the α phase precipitation is a diffusion-type transformation. The crystal defects (e. g. dislocations) and grain boundaries will become preferentially heterogeneous nucleation sites for α phase [30]. In the CR specimen, the large amounts of crystal defects and sub-grains are reserved and can provide numerous nucleation sites for α phase. The high concentration of defects in the CR specimen also reduces the energy barrier for the nucleation of α phase [33]. Therefore, the α precipitated in the CRA-573 specimen even at a lower aging temperature of 573 K. In general, α phase particles are bounded by a combination of coherent or semi-coherent facets and incoherent interfaces to minimize the total interfacial free energy [34]. The incoherent interfaces migrate much faster than the coherent or semi-coherent interfaces, leading to the formation of the acicular α phase in the STA-773 specimens [35]. On the other hand, the formation of the equiaxed α phase in CRA-773 specimen may be due to the fact that only one interface is coherent or semi-coherent and the other interfaces are incoherent which can migrate much faster [12]. Similar phenomena of the ultrafine equiaxed α phase has been observed in other metastable β Ti alloys during aging after plastic deformation [36, 37]. The formation of α phase PFZ along the grain boundary observed in Fig. 3(d) is related to elements diffusion. Due to the preferential precipitation of α phases at grain boundaries, the elements segregation occurs. The α stabilizing O element diffuses from the adjacent regions into α phase and the β stabilizing elements (such as Nb) diffuse from α phase into the adjacent regions. Consequently, the β phase of the adjacent regions is subsequently stabilized, which can prevent the precipitation of other α phase and the FPZ appears.

The results show here conclusively show that different microstructural conditions depend on the variation in process history. The key factors are high-density dislocations and grain boundaries induced by CR, which promote the precipitation of α phase and suppress the formation of ω phase during aging.

Strengthening mechanisms

Previous studies have shown that the deformation mechanisms of β-Ti alloys depend on the β stability [38]. The precipitation of ω phase results in the diffusion of β-stabilizing elements into the adjacent β matrix, resulting in enhancing the stability of the β matrix [39]. For the STA-573 specimen, the stress-induced martensitic transformation occurring in the ST specimens disappeared, i.e., the double yielding behavior disappeared in the strain–stress curves, resulting from the ω precipitates as shown in Fig. 4(b). Previously, the ω phase was considered to be a nondeformable precipitate in the isothermal treated β-Ti alloys, which could block the dislocation motion and derive precipitate hardening mechanisms [40]. Due to the difference in shear modulus between β and ω phase, the modulus hardening ($\Delta\tau$) can be used to calculated the ω-induced increase in the critical resolved shear stress for dislocation [40]. According to the literature [41], the yield strength of materials containing nano-sized and small-content precipitated phase can be roughly calculated by $\sigma_y = s_0 + M\Delta t$ and $\Delta\tau$ can be expressed as,

$$\Delta\tau = 0.9\sqrt{rf}\frac{T}{b}\left\{\frac{G_\omega - G_\beta}{G_\beta}\frac{1}{2b\ln(l_\omega/b)}\right\}^{2/3}$$

In the formula, T is the dislocation line tension, which is approximated by $G_\beta b^2/2$ and b is the magnitude of the Burgers vector of the $a_\beta/2<111>$ dislocation. G_ω and G_β is the shear modulus of ω and β phase, respectively. In this work, the shear modulus G_ω and G_β are estimated to be 12.20 GPa and 26.99 GPa, respectively from elastic properties of the Ti-25 at.% Nb alloy [42]. According to the dark-field TEM image [Fig. 4(b)], the mean particle size d_0 is around 3.4 ± 0.73 nm and the average radius r is around 1.7 nm. Figure 8 shows the size distribution of the ω particles. The number density of ω particles, n, is about 1.3×10^{-3}/nm^3. The interparticle spacing l_ω and the volume fraction f of ω particles are calculated by $l = 1/\sqrt{2d_0 n}$ and $f = pnd_0^3/6$, respectively [40]. After the calculation, finally, the l_ω and f can be confirmed 10.9 ± 1.12 nm and ~2.2 ± 0.09%. M is an average Taylor factor of 2.754 for the present polycrystalline material [43]. Here, the calculated result for $\Delta\tau$ is 234 MPa and thus $M\Delta\tau$ can be confirmed to be 645 MPa. This indicates that ω phase plays an important role in strengthening the mechanical response. Meanwhile, the σ_0 is roughly 353 MPa, which is between the first yield point (stress-induced martensitic transformation) and the second yielding point (dislocation slip) observed in Fig. 6. And between the two-yield point, the stress-induced α'' martensite plates act as obstacles against dislocation motion and thus reduce the dislocation mean free path, resulting in the dynamic Hall–Petch effect [40,

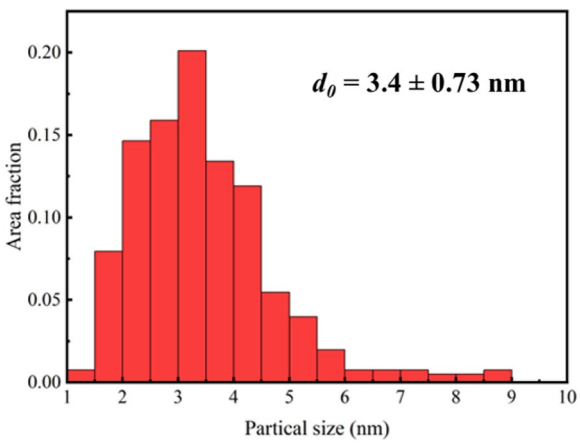

Figure 8: Size distribution of the ω particles shown in Fig. 4(b).

44]. The ω precipitates also result in high Young's modulus of the STA-573 specimen. In contrast, the CRA-573 specimen is notably reinforced due to the inhibitory effects of dislocation tangles, grain boundaries, and α precipitates. And the modulus of the CRA-573 specimen is relatively low due to the absence of ω phase.

The different mechanical properties of the CRA-773 and STA-773 specimens are related to the different morphology and volume fraction of α phases in β matrix. The precipitate of the α phases into the β matrix improves the tensile strength as a result of precipitation strengthening. The plastic deformation preferentially occurs in the β matrix and the α/β interfaces can hinder dislocation movement, due to the higher hardness of the α phase [12]. On the other hand, the precipitation of α phase will lead to the β-stabilizer such as Nb enriched in β matrix and thus result in an increased β-stability. In addition, the α precipitates decrease β domain size resulting in fine-grain strengthening. The above-mentioned reasons together lead to an increase in strength of the STA-773 and CRA-773 specimens compared with the ST specimen. In CRA-773 specimen, the volume fraction of the α phase is higher, which leads to higher β stability of the retained β matrix. Besides, the β domain size of the CRA-773 specimen is decreased down to nano-scale by dispersed nano-scaled α phase. While in the STA-773 specimen, the PFZ with micro-scale size can be observed. The equiaxed α phase is harder than the acicular α phase [45]. Therefore, the CRA-773 specimen shows higher strength than the STA-773 specimen due to the ultrafine equiaxed α phase. The STA-773 specimen exhibits nonlinear elasticity, which is an intermediate stage between "double yielding" and normal linear elasticity and has relatively good plasticity. Figure 9 shows the XRD profiles of the CRA-773 and STA-773 specimens after deformation. In addition to α and β phases, the peaks of α'' phase can be observed in STA-773 specimen after deformation. This means that the remaining stress-induced β to α'' transformation is triggered by the applied stress in the STA-773 specimen. On the contrary, only α and β phase diffraction peaks can be found in CRA-773 specimen. It is evident that the higher β stability and ultrafine β domain can suppress stress-induced martensitic transformation during tension [38]. In the STA-773 specimen, the critical stress for SIM increases and has a similar value to the critical stress of dislocation slip, which leads to nonlinear elasticity. However, the stress-induced β to α'' transformation is completely inhibited in the CRA-773 specimen due to the higher β stability and ultrafine β domain.

Conclusions

The effects of CR on the α and ω precipitations during aging treatment and corresponding mechanical properties of metastable Ti–38Nb–0.2O alloy were systematically investigated in this study. The results can be summarized as follows.

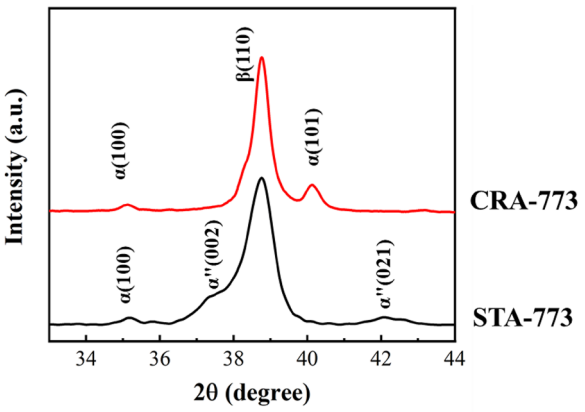

Figure 9: XRD profiles of the STA-773 and CRA-773 specimens after deformation.

(1) Due to the low β stability, the Ti–38Nb–0.2O alloy with a single β phase exhibits stress-induced martensitic transformation during cold deformation. And a swirled marble-like microstructure is visible in CR specimens.

(2) Even under the same aging temperature, the microstructure evolution could be different, depending on the pre-treatment prior aging. The results mainly are attributed to the high-density dislocations and grain boundaries introduced by CR, which suppress the formation of ω phase and PFZ, and promote the precipitation of α phase. Meanwhile, the dispersed nanoscaled α phase was achieved by aging at 773 K in CR specimens.

(3) The ω precipitates could retard the dislocation motion and derive precipitate hardening mechanisms, which greatly strengthen the specimen. And the strengthening effect of ω phase is better than that of α phase. The precipitates of α or ω both suppress the stress-induced α'' transformation.

(4) The STA-773 specimen shows peculiar nonlinear deformation behavior. The CRA-573 specimen is significantly strengthened and exhibits high UTS (1102 MPa) and relatively low Young's modulus (60 GPa).

Materials and methods

The Ti–38Nb–0.2O ingot was prepared by vacuum arc melting using pure Ti, pure Nb, and TiO_2. The Ti and Nb contents were analyzed using an inductively coupled plasma (ICP) method. The oxygen content was determined using an inert gas fusion-infrared absorption method. The actual composition of this alloy after melting is Ti-37.98Nb-0.183O. To ensure the macroscopic homogeneity of the elements, the ingot was melted for 5 times and then homogenized at 1273 K for 7.2 ks followed by water quenching. The homogenized ingot was cold-rolled into 1.5 mm

thin plates corresponding to an 85% reduction of the original thickness. This condition will be referred to as the cold-rolled (CR) state. Some of the CR specimens were solution-treated (ST) at 1173 K for 30 min to undergo recrystallization and followed by water quenching to obtain a single β microstructure at room temperature, referred to as ST state. The ST and CR specimens were respectively aged at 573 K and 773 K for 2 h. The aged specimens were named by initial treatment and aging temperature, such as CRA-573, CRA-773, STA-573 and STA-773. The above-mentioned heat treatments were carried out in the Ar gas atmosphere to avoid oxidation and cooled by water quenching.

The mechanical properties were evaluated on Instron 8801 machine at room temperature at a strain rate of 4×10^{-4} s^{-1}. All tensile tests were performed along the rolling direction. The phase constitution was identified by the X-ray diffraction (XRD, D/MAX-2500) with Cu Kα irradiation at a current of 250 mA and an accelerating voltage of 40 kV. The microstructures were characterized by optical microscopy (OM, LEICA DM4000), scanning electron microscopy (SEM, Apreo S LoVac), and transmission electron microscopy (TEM, JEM-2100F). The TEM specimen was prepared by a conventional twin-jet polishing method with a solution of hydrofluoric acid: sulfuric acid: methanol = 2:5:93 in volume at 233 K.

Acknowledgments

The authors gratefully acknowledge the funding of the National Natural Science Foundation of China (NSFC, No. 51671012) and the National Natural Science Foundation of China (NSFC, No.52001018).

Data availability

The datasets generated during and/or analyzed during the current study are available from the corresponding author on reasonable request.

Code availability

Not applicable.

Declarations

Conflict of interest On behalf of all authors, the corresponding author states that there is no conflict of interest.

References

1. D. Banerjee, J.C. Williams, Perspectives on titanium science and technology. Acta Mater. **61**(3), 844 (2013)
2. M. Bonisch, M. Calin, J. van Humbeeck, W. Skrotzki, J. Eckert, Factors influencing the elastic moduli, reversible strains and hysteresis loops in martensitic Ti–Nb alloys. Mater. Sci. Eng. C Mater. Biol. Appl. **48**, 511 (2015)
3. J.Y. Zhang, G.F. Chen, Y.Y. Fu, Y. Fan, Z. Chen, J. Xu, H. Chang, Z.H. Zhang, J. Zhou, Z. Sun, B.L. Shen, F. Sun, Strengthening strain-transformable β Ti-alloy via multi-phase nanostructuration. J. Alloy. Compd. **799**, 389 (2019)
4. F. Sun, Y.L. Hao, J.Y. Zhang, F. Prima, Contribution of nano-sized lamellar microstructure on recoverable strain of Ti–24Nb–4Zr–7.9Sn titanium alloy. Mater. Sci. Eng. A **528**(25–26), 7811 (2011)
5. W. Chen, S. Cao, W. Kou, J. Zhang, Y. Wang, Y. Zha, Y. Pan, Q. Hu, Q. Sun, J. Sun, Origin of the ductile-to-brittle transition of metastable β-titanium alloys: self-hardening of ω-precipitates. Acta Mater. **170**, 187 (2019)
6. J.W. Foltz, B. Welk, P.C. Collins, H.L. Fraser, J.C. Williams, Formation of grain boundary α in β Ti alloys: its role in deformation and fracture behavior of these alloys. Metall. Mater. Trans. A **42**(3), 645 (2010)
7. Y. Fu, W. Xiao, J. Wang, L. Ren, X. Zhao, C. Ma, A novel strategy for developing α + β dual-phase titanium alloys with low young's modulus and high yield strength. J. Mater. Sci. Technol. **76**, 122–128 (2020)
8. E.M. Hildyard, L.D. Connor, L.R. Owen, D. Rugg, N. Martin, H.J. Stone, N.G. Jones, The influence of microstructural condition on the phase transformations in Ti–24Nb (at.%). Acta Mater. **199**, 129 (2020)
9. H. Wang, S.-W. Xin, Y.-Q. Zhao, W. Zhou, W.-D. Zeng, Forging–microstructure–tensile properties correlation in a new near β high-strength titanium alloy. Rare Met. **40**(8), 2109 (2020)
10. D.L. Moffat, D.C. Larbalestier, The compctition between the alpha and omega phases in aged Ti–Nb alloys. Metall. Trans. A **19**(7), 1687 (1988)
11. A. Berg, J. Kiese, L. Wagner, Microstructural gradients in Ti–3Al–8V–6Cr–4Zr–4Mo for excellent HCF strength and toughness. Mater. Sci. Eng. A **243**(1), 146 (1998)
12. B. Jiang, S. Emura, K. Tsuchiya, Microstructural evolution and its effect on the mechanical behavior of Ti–5Al–5Mo–5V–3Cr alloy during aging. Mater. Sci. Eng. A **731**, 239 (2018)
13. S. Guo, Q. Meng, G. Liao, L. Hu, X. Zhao, Microstructural evolution and mechanical behavior of metastable β-type Ti–25Nb–2Mo–4Sn alloy with high strength and low modulus. Prog. Nat. Sci. Mater. Int. **23**(2), 174 (2013)
14. S. Guo, Q. Meng, L. Hu, G. Liao, X. Zhao, H. Xu, Suppression of isothermal ω phase by dislocation tangles and grain boundaries in metastable β-type titanium alloys. J. Alloy. Compd. **550**, 35 (2013)
15. S. Guo, Z. Bao, Q. Meng, L. Hu, X. Zhao, A novel metastable Ti–25Nb–2Mo–4Sn alloy with high strength and low young's modulus. Metall. Mater. Trans. A **43**(10), 3447 (2012)
16. M. Yan, W. Xu, M.S. Dargusch, H.P. Tang, M. Brandt, M. Qian, Review of effect of oxygen on room temperature ductility of titanium and titanium alloys. Powder Metall. **57**(4), 251 (2014)

17. J.I. Kim, H.Y. Kim, H. Hosoda, S. Miyazaki, Shape memory behavior of Ti–22Nb–(0.5–2.0) O (at%) biomedical alloys. Mater. Trans. **46**(4), 852 (2005)
18. T. Saito, T. Furuta, J.H. Hwang, S. Kuramoto, K. Nishino, N. Suzuki, R. Chen, A. Yamada, K. Ito, Y. Seno, T. Nonaka, H. Ikehata, N. Nagasako, C. Iwamoto, Y. Ikuhara, T. Sakuma, Multifunctional alloys obtained via a dislocation-free plastic deformation mechanism. Science **300**(5618), 464 (2003)
19. Y.L. Hao, Z.B. Zhang, S.J. Li, R. Yang, Microstructure and mechanical behavior of a Ti–24Nb–4Zr–8Sn alloy processed by warm swaging and warm rolling. Acta Mater. **60**(5), 2169 (2012)
20. S. Hanada, N. Masahashi, T.K. Jung, Effect of stress-induced α″ martensite on Young's modulus of β Ti–33.6Nb–4Sn alloy. Mater. Sci. Eng. A **588**, 403 (2013)
21. C.M. Liu, H.M. Wang, X.J. Tian, H.B. Tang, Subtransus triplex heat treatment of laser melting deposited Ti–5Al–5Mo–5V–1Cr–1Fe near β titanium alloy. Mater. Sci. Eng. A **590**, 30 (2014)
22. J.I. Qazi, V. Tsakiris, B. Marquardt, H.J. Rack, Effect of aging treatments on the tensile properties of Ti–35Nb–7Zr–5Ta–(00.6–0.7)O alloys. J. ASTM Int. **2**(8), 12780 (2005)
23. J.I. Kim, H.Y. Kim, T. Inamura, H. Hosoda, S. Miyazaki, Effect of annealing temperature on microstructure and shape memory characteristics of Ti–22Nb–6Zr(at%) biomedical alloy. Mater. Trans. **47**(3), 505 (2006)
24. W.-T. Qu, H. Gong, J. Wang, Y.-S. Nie, Y. Li, Martensitic transformation, shape memory effect and superelasticity of Ti–xZr–(30–x)Nb–4Ta alloys. Rare Met. **38**(10), 965 (2019)
25. Q. Meng, S. Guo, Q. Liu, L. Hu, X. Zhao, A β-type TiNbZr alloy with low modulus and high strength for biomedical applications. Prog. Nat. Sci. Mater. Int. **24**(2), 157 (2014)
26. M. Tahara, H.Y. Kim, T. Inamura, H. Hosoda, S. Miyazaki, Role of interstitial atoms in the microstructure and non-linear elastic deformation behavior of Ti–Nb alloy. J. Alloy. Compd. **577**, S404 (2013)
27. Y.L. Hao, S.J. Li, S.Y. Sun, C.Y. Zheng, Q.M. Hu, R. Yang, Superelastic titanium alloy with unstable plastic deformation. Appl. Phys. Lett. **87**(9), 091906 (2005)
28. J.P. Cui, Y.L. Hao, S.J. Li, M.L. Sui, D.X. Li, R. Yang, Reversible movement of homogenously nucleated dislocations in a beta-titanium alloy. Phys Rev Lett. **102**(4), 045503 (2009)
29. T. Furuta, S. Kuramoto, J. Hwang, K. Nishino, T. Saito, Elastic deformation behavior of multi-functional Ti–Nb–Ta–Zr–O Alloys. Mater. Trans. **46**(12), 3001 (2005)
30. S. Nag, R. Banerjee, R. Srinivasan, J.Y. Hwang, M. Harper, H.L. Fraser, ω-Assisted nucleation and growth of α precipitates in the Ti–5Al–5Mo–5V–3Cr–0.5Fe β titanium alloy. Acta Mater. **57**(7), 2136 (2009)
31. L.M. Hsiung, D.H. Lassila, Shock-induced deformation twinning and omega transformation in tantalum and tantalum–tungsten alloys. Acta Mater. **48**(20), 4851 (2000)
32. T. Richeton, J. Weiss, F. Louchet, Dislocation avalanches: role of temperature, grain size and strain hardening. Acta Mater. **53**(16), 4463 (2005)
33. B. Jiang, S. Emura, K. Tsuchiya, Formation of equiaxed α phase in Ti–5Al–5Mo–5V–3Cr alloy deformed by high-pressure torsion. J. Alloy. Compd. **738**, 283 (2018)
34. S. Zherebtsov, G. Salishchev, S. Lee Semiatin, Loss of coherency of the alpha/beta interface boundary in titanium alloys during deformation. Philos. Mag. Lett. **90**(12), 903 (2010)
35. T. Furuhara, T. Makino, Y. Idei, H. Ishigaki, A. Takada, T. Maki, Morphology and crystallography of α precipitates in β Ti–Mo binary alloys. Mater. Trans. **39**(1), 31 (1998)
36. A. Zafari, K. Xia, Formation of equiaxed α during ageing in a severely deformed metastable β Ti alloy. Scripta Mater. **124**, 151 (2016)
37. K. Bartha, J. Stráský, A. Veverková, P. Barriobero-Vila, F. Lukáč, P. Doležal, P. Sedlák, V. Polyakova, I. Semenova, M. Janeček, Effect of the high-pressure torsion (HPT) and subsequent isothermal annealing on the phase transformation in biomedical Ti15Mo alloy. Metals **9**(11), 1194 (2019)
38. M. Ahmed, D. Wexler, G. Casillas, O.M. Ivasishin, E.V. Pereloma, The influence of β phase stability on deformation mode and compressive mechanical properties of Ti–10V–3Fe–3Al alloy. Acta Mater. **84**, 124 (2015)
39. S.A. Mantri, D. Choudhuri, T. Alam, V. Ageh, F. Sun, F. Prima, R. Banerjee, Change in the deformation mode resulting from beta-omega compositional partitioning in a Ti Mo alloy: room versus elevated temperature. Scripta Mater. **130**, 69 (2017)
40. M.J. Lai, T. Li, D. Raabe, ω phase acts as a switch between dislocation channeling and joint twinning- and transformation-induced plasticity in a metastable β titanium alloy. Acta Mater. **151**, 67 (2018)
41. A. Melander, P.Å. Persson, The strength of a precipitation hardened AlZnMg alloy. Acta Metall. **26**(2), 267 (1978)
42. J. Sun, Q. Yao, H. Xing, W.Y. Guo, Elastic properties of β, α″ and ω metastable phases in Ti–Nb alloy from first-principles. J. Phys. Condens. Matter **19**(48), 486215 (2007)
43. J.M. Rosenberg, H.R. Piehler, Calculation of the Taylor factor and lattice rotations for bcc metals deforming by pencil glide. Metall. Trans. **2**(1), 257 (1971)
44. N. Chen, H. Kou, Z. Wu, F. Qiang, C. Wang, J. Li, J.M. Molina-Aldareguia, Stress-induced α″ martensitic phase transformation and martensitic twinning in a metastable β titanium alloy. J. Alloys Compd. **859**, 157809 (2021)
45. J. Dong, F. Li, C. Wang, Micromechanical behavior study of α phase with different morphologies of Ti–6Al–4V alloy by microindentation. Mater. Sci. Eng. A **580**, 105 (2013)